

CO impurities effect on LaNi_{4.7}Al_{0.3} hydrogen storage alloy hydrogenation/dehydrogenation properties

QI WAN¹, PING LI^{1*}, YUNLONG LI¹, FUQIANG ZHAI¹, WEINA ZHANG¹, LIQUN CUI¹, ALEX A VOLINSKY³ and XUANHUI QU^{1,2}

¹Institute for Advanced Materials and Technology, University of Science and Technology, Beijing, Beijing 100083, China

²State Key Laboratory for Advanced Metals and Materials, University of Science and Technology, Beijing, Beijing 100083, China

³Department of Mechanical Engineering, University of South Florida, Tampa, FL 33620, USA

MS received 27 February 2013

Abstract. LaNi_{4.7}Al_{0.3} alloy was prepared by vacuum induction melting in high purity helium atmosphere, and the ingot was pulverized into 200–400 mesh powder after annealing. X-ray diffraction (XRD) and scanning electron microscopies (SEM) were utilized to study the alloy morphology and phase structure. X-ray photoelectron spectroscopy (XPS) was used for surface analysis. The poisoned alloy was tested at 30 °C in the mixture gas by thermogravimetric and differential thermal analyses (TG + DTA). The hydrogen storage properties were studied by the pressure–composition–temperature test. The activated sample was completely deactivated after only 3 hydriding/dehydriding cycles in hydrogen containing 300 ppm CO at 30 °C, but hydrogen storage capacity did not degrade when tested at 80 °C. Additionally, two different steps appeared in the absorption processes. Combined with XRD, XPS and TG + DTA results, an explanation for this phenomenon is given.

Keywords. LaNi_{4.7}Al_{0.3} hydrogen storage alloy; CO impurities gas; hydrogen purification; absorption/desorption kinetics.

1. Introduction

Hydrogen energy attracts worldwide attention due to the growing shortage of traditional energy sources and environmental pollution. In order to efficiently utilize energy from hydrogen, it needs to be separated from the mixed gases. At present, there are several reports on separation and purification of hydrogen from mixed gases (Sheridan III *et al* 1983; Au *et al* 1996; Tosti *et al* 2000; Ibeh *et al* 2007; Tagliabue and Delnero 2008; Cássia Colman *et al* 2009; Majlan *et al* 2009; Mendes *et al* 2010; David and Kopac 2011; Hwang *et al* 2011; Kosmambetova *et al* 2011; Miura *et al* 2012). Selective hydrogen absorption by hydriding alloys, which can reversibly absorb/desorb hydrogen, offers the possibility of hydrogen separation from the mixed gases and hydrogen purification to the ultra-high levels.

AB₅-type hydrogen storage alloy is one of the most promising hydrogen storage materials. It has the largest hydrogen storage capacity and the highest hydriding reaction rate at room temperature and medium pressure, compared with other hydrogen storage materials (Van Vucht *et al* 1970). However, the reaction rates and the hydrogen

storage capacity of AB₅-type alloys can be profoundly affected by various impurities present in hydrogen gas, even at low concentration levels (Goodell 1983). The performance characteristics of hydrogen storage alloys can be poisoned by the slow absorption/desorption rates, which decrease hydrogen absorption capacity. In order to utilize AB₅-type hydrogen storage alloy for hydrogen separation and purification in the future, it is necessary to study hydrogen absorption and desorption kinetics performance in mixed gases.

Sandrock and Goodell (1980) first studied the surface poisoning of LaNi₅ by O₂, CO and H₂O, and found that CO contamination seems to be the most harmful for LaNi₅. Therefore, studying CO poisoning of AB₅-type hydrogen storage alloys is quite significant. In the past years, there have been numerous reports of the poisoning mechanism in AB₅-type hydrogen storage alloys (Sandrock and Goodell 1980, 1984; Eisenberg and Goodell 1983; Goodell 1983; Han and Lee 1989; Imoto *et al* 1995; Sakaguchi *et al* 1995; Scura *et al* 2008; Dunikov *et al* 2012). In order to improve resistance to CO and other impurities, surface modification has also been considered (Wang *et al* 1995; Uchida 1999; Sun and Suda 2002; Williams *et al* 2009a, b; Ren *et al* 2010; Lototsky *et al* 2011; Zhao *et al* 2011).

*Author for correspondence (ustbplping@126.com)

Although researches have considered LaNi_5 performance in CO impurity gas, some of the poisoning mechanisms are still unclear, with even less emphasis on the $\text{LaNi}_{4.7}\text{Al}_{0.3}$ alloy. On the other hand, Al can substitute Ni in LaNi_5 , resulting in a much lower decomposition pressure, without impairing kinetics or hydrogen storage capacity (Mendelsohn *et al* 1977). At the same time, $\text{LaNi}_{4.7}\text{Al}_{0.3}$ has better CO tolerance compared with LaNi_5 (Han and Lee 1989), which prompted researching $\text{LaNi}_{4.7}\text{Al}_{0.3}$ alloy for hydrogen storage. In this paper, hydrogenation kinetics of $\text{LaNi}_{4.7}\text{Al}_{0.3}$ at 30 and 80 °C is compared. Hydrogenation performance in the mixture gas of $\text{H}_2 + 300$ ppm CO at 80 °C is better than that of at 30 °C. When extending the absorption and desorption time, two steps in the absorption curves during the hydriding/dehydriding cycle are reported for the first time. Based on the published theories, experimental results of this paper are explained, and the corresponding poisoning mechanism is identified.

2. Experimental

$\text{LaNi}_{4.7}\text{Al}_{0.3}$ alloy was prepared by vacuum inductive melting in the high purity helium atmosphere. The ingot was pulverized into 200–400 mesh powder after 1150 °C annealing for 25 h. The purity of as-received metals, including lanthanum, nickel and aluminum, using commercial ingots as raw materials, was above 99.99%.

The phase structure of the powders before and after the experiments were characterized by XRD (X'pert-MPD, Philips) using $\text{CuK}\alpha$ radiation and the morphology of the powders was examined by SEM. The XRD scan rate was set at 1 s per step of 0.02° (2θ), and the range of all measurements was restricted to $10\text{--}80^\circ$ (2θ). X-ray photoelectron spectroscopy (XPS) was performed using AXIS Ultra DLD (Kratos Analytical, Japan). Simultaneous DTA and TG analyses were conducted using NETZSCH STA 449C system (Netzsh, Germany). Heating runs was performed at the rate of $5^\circ\text{C}/\text{min}$ from 30 to 150 °C.

Hydrogen storage properties were measured by an isovolumetric method using pressure–composition–temperature apparatus (Xie *et al* 2009). The sample activation was performed at 100 °C under 3 MPa and then cycled 8 times at 30 and 80 °C under the initial pressure, and then tested in the mixed gases. All desorption experiments were carried out in vacuum.

3. Results and discussion

3.1 Microstructural analysis

Figure 1 shows SEM micrographs of the $\text{LaNi}_{4.7}\text{Al}_{0.3}$ alloy before and after the cycling. The particle size of the powder after the cycling is smaller due to pulverization.

Figure 2 shows XRD patterns of the $\text{LaNi}_{4.7}\text{Al}_{0.3}$ alloy after cycling ((a) in pure H_2 at 80 °C; (b) in impure H_2 at 80 °C and (c) in impure H_2 at 30 °C). When cycled in pure and impure H_2 at 80 °C, the same LaNi_5 main phase remained, which is why the ultimate hydrogen capacity did not decrease. When cycled in impure H_2 at 30 °C, the same LaNi_5 main phase remained, accompanied by the undecomposed LaNi_5H_6 phase presence. The presence of the LaNi_5H_6 phase indicates that CO hinders the dehydrogenation process, which results in the hydrogen absorption capacity decline after 30 °C cycling.

3.2 Absorption/desorption kinetics

Figure 3 shows absorption/desorption kinetics curves of $\text{LaNi}_{4.7}\text{Al}_{0.3}$ alloy at 80 °C in pure H_2 . It can be seen that no change in hydrogen transfer capacity and hydriding/dehydriding rates happened after 16 cycles. Figure 4 shows the absorption kinetics curves of $\text{LaNi}_{4.7}\text{Al}_{0.3}$ alloy at 30 °C in impure H_2 . It can be seen from figure 4 that dynamics and hydrogen absorption capacity of the activated $\text{LaNi}_{4.7}\text{Al}_{0.3}$ sample did not change after 8 cycles in

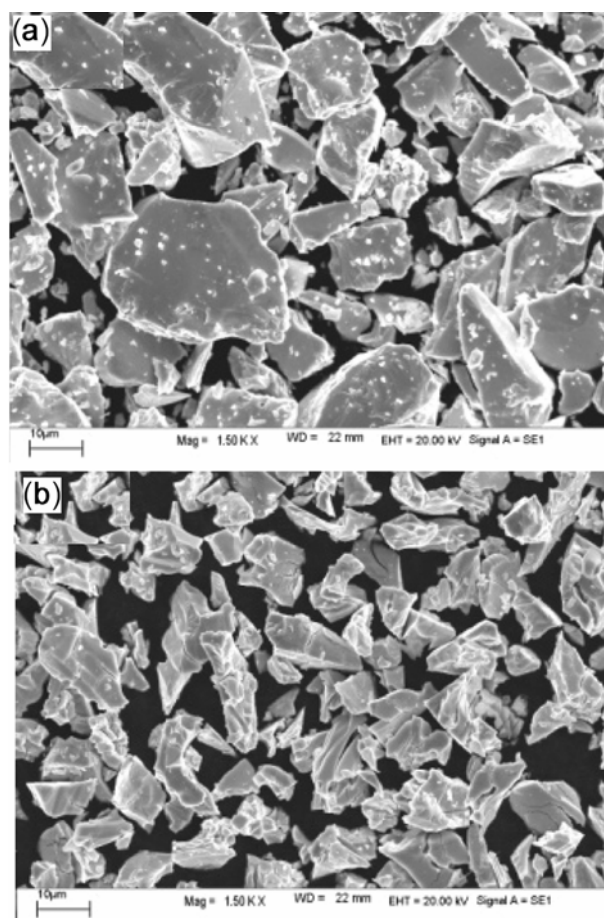


Figure 1. SEM micrographs of $\text{LaNi}_{4.7}\text{Al}_{0.3}$ alloy (a) before cycling and (b) after cycling.

pure hydrogen. However, the sample could not absorb hydrogen after only 3 cycles in mixed $\text{H}_2 + 300$ ppm CO gases.

Figure 5 shows desorption kinetics curves of $\text{LaNi}_{4.7}\text{Al}_{0.3}$ alloy at 30°C in impure H_2 . Only the first 40 min of the curves should be considered, because the desorption rate becomes very slow after mixed gases cycling. It can be seen from figure 5 that the alloy desorbed hydrogen completely within 5 min, when cycled in pure H_2 . There is incomplete desorption even after 40 min of the impure H_2 cycling.

Figure 6 shows absorption kinetics curves of the $\text{LaNi}_{4.7}\text{Al}_{0.3}$ alloy at 80°C in impure H_2 . It can be seen from figure 6 that kinetic properties and hydrogen absorption capacity of the activated sample did not

change after 8 cycles in pure hydrogen (curves 1–8). Then, the sample was cycled 7 times in the gas mixture (curves 9–15). When tested in impure H_2 at 80°C , the sample exhibited some interesting properties. Hydrogen absorption capacity did not decay when compared with the 30°C test. The absorption curves can be divided into two steps. The first step exhibits slower absorption rate, while the second is the rapid hydrogenation rate step and it takes longer time to complete the first step with the number of cycles.

Figure 7 shows desorption kinetics curves of $\text{LaNi}_{4.7}\text{Al}_{0.3}$ alloy at 80°C in impure. Only the first 60 min of the curves are considered. When tested in pure H_2 , the desorption rate is very fast and hydrogen desorption is completed within 5 min. However, when tested in mixed gases, desorption rate slows down and requires longer time for the complete desorption with increasing the number of cycles.

The major viewpoints of the mechanism of hydrogen confinement in LaNi_5 using CO poisoning are as follows. Wallace *et al* (1979) reported that the surface of LaNi_5 exposed to air consists of the $\text{La}(\text{OH})_3$ layer with precipitated Ni, and hydrogen molecules are dissociated into

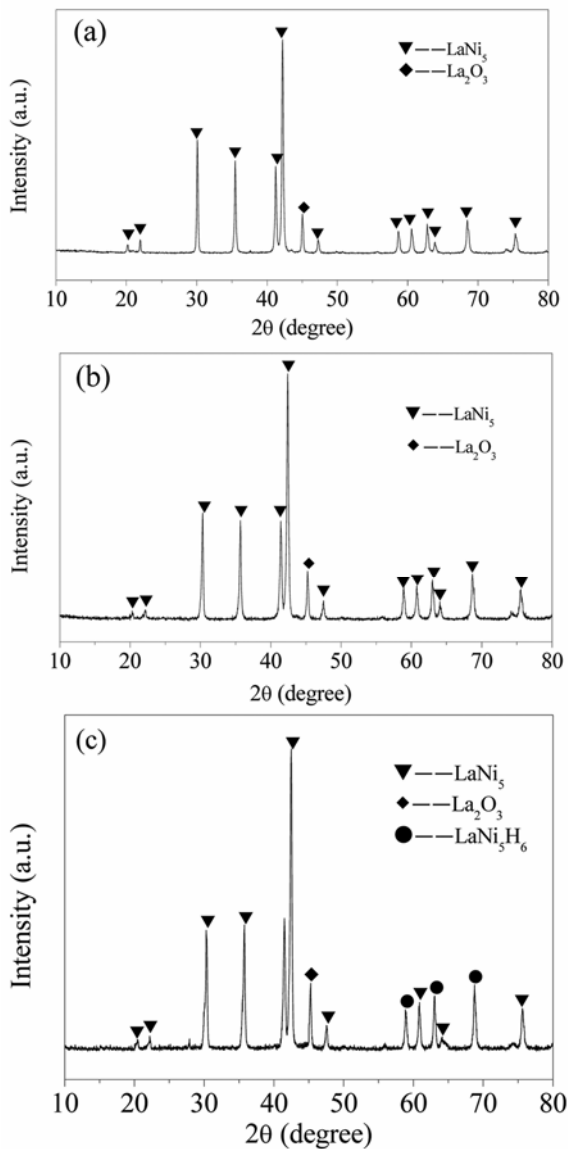


Figure 2. XRD patterns of $\text{LaNi}_{4.7}\text{Al}_{0.3}$ alloy (a) in pure H_2 at 80°C ; (b) in impure H_2 at 80°C and (c) in impure H_2 at 30°C .

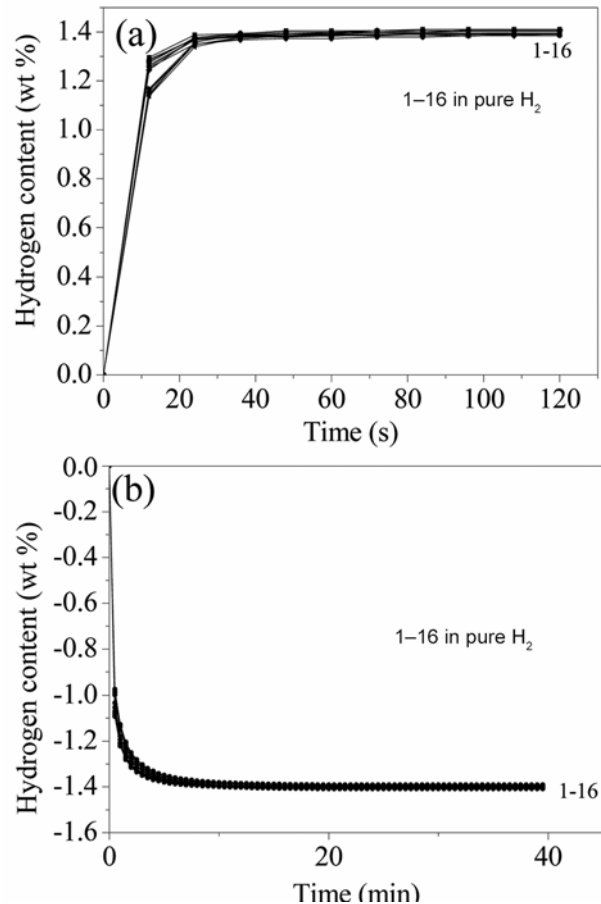


Figure 3. Absorption/desorption kinetics curves of $\text{LaNi}_{4.7}\text{Al}_{0.3}$ alloy at 80°C in pure H_2 (a) absorption and (b) desorption.

hydrogen atoms on the Ni sites. Schlapbach *et al* (1980) suggested that the segregation occurs on the LaNi_5 surface owing to La oxidation and Ni clusters precipitation, and the Ni clusters act as a catalyst for hydrogenation. Sakaguchi *et al* (1995) claimed that CO molecules preferentially absorb metallic Ni precipitated on the surface of hydrogenated LaNi_5 , and replace chemisorbed hydrogen atoms, owing to higher adsorptive activity of CO in comparison with hydrogen. Although, the poisoning mechanism is complicated and not uniform, metallic Ni on the surface appears to play an important role in hydrogenation processes.

The hydrogenation/dehydrogenation phenomenon is different in pure hydrogen and impure hydrogen, which can be explained by the role of metallic Ni on the surface of samples. When $\text{LaNi}_{4.7}\text{Al}_{0.3}$ alloy cycled at 30 °C in $\text{H}_2 + 300 \text{ ppm CO}$, CO molecules absorb on metallic Ni

precipitated on the surface, and replace chemisorbed hydrogen atoms. Thus, hydrogenation process is confined because of the adsorbed CO molecules. On the other hand, hydrogen desorbed in each cycle is not completely due to the adsorbed CO molecules. Large quantities of absorbed hydrogen are accumulated in $\text{LaNi}_{4.7}\text{Al}_{0.3}$ with repeated cycling, and the accumulation of hydrogen causes the amount of hydrogen absorbed in the next cycle to be decreased. The XRD results confirm this.

The reason for hydrogen absorption capacity and absorption rate decline at 80 °C is the same as for the 30 °C cycling. Namely, the adsorbed CO molecules confined the hydrogenation process, which corresponds to the first step of the hydrogen absorption curves. CO chemisorption on Ni surface will take some time to complete, which depends on Ni and CO content, and, to some extent, on temperature and pressure.

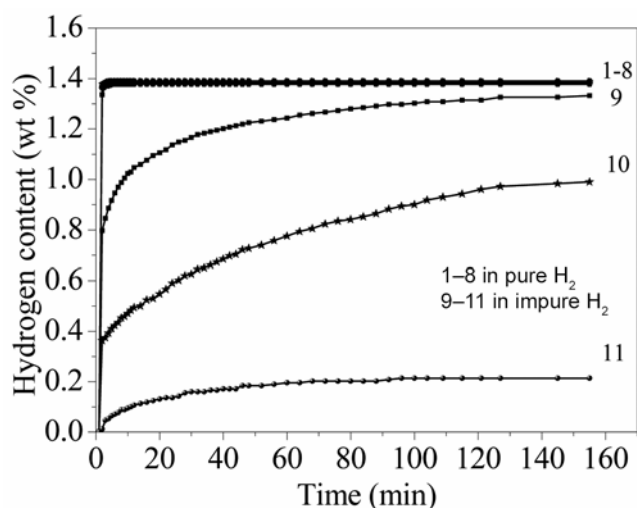


Figure 4. Absorption kinetics curves of $\text{LaNi}_{4.7}\text{Al}_{0.3}$ alloy at 30 °C in impure H_2 .

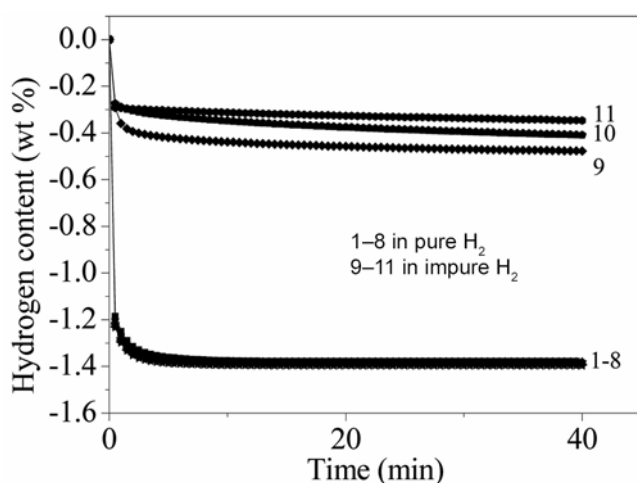


Figure 5. Desorption kinetics curves of $\text{LaNi}_{4.7}\text{Al}_{0.3}$ alloy at 30 °C in impure H_2 .

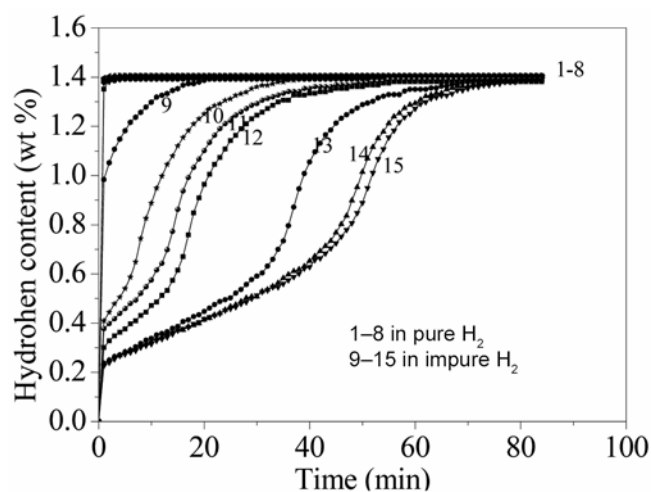


Figure 6. Absorption kinetics curves of $\text{LaNi}_{4.7}\text{Al}_{0.3}$ alloy at 80 °C in impure H_2 .

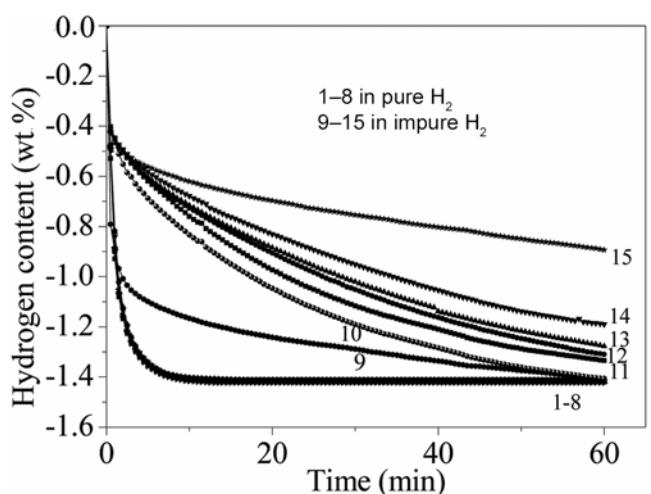


Figure 7. Desorption kinetics curves of $\text{LaNi}_{4.7}\text{Al}_{0.3}$ alloy at 80 °C in impure H_2 .

Since CO causes uneven surface deactivation, only a handful of alloy particles are affected in the beginning, resulting in a rapid hydrogenation rate, as seen in figure 5 (curve 9). However, more alloy particles are affected by the introduction of new CO impurities after each cycle. We know that metallic Ni preferentially adsorbs CO, while Ni acts as a catalyst in the $\text{H}_2 \rightarrow 2\text{H}$ process. Since CO occupies active sites, hydrogen absorption properties declined. On the other hand, more Ni-rich precipitation clusters are formed on the surface with each cycle (Schlapbach *et al* 1980). Ni clusters precipitation can promote rapid decomposition of hydrogen molecules into atoms, along with CO adsorption. When CO chemisorption process achieves equilibrium, the remaining Ni on the surface will quickly cause hydrogen molecules decomposition into atoms, showing rapid hydrogenation rate. In addition, the particle size in the second step is smaller than that of the first step due to pulverization, while smaller particle size also seems to have a certain contribution to the rapid hydrogenation rate, since smaller particles have faster kinetics compared with the larger ones (Corré *et al* 1997). From the above analysis, it is clear that the second step has faster absorption rate compared with the first step, as seen in figure 6.

3.3 XPS results

XPS was performed to test for Ni, an important element in hydrogen absorption and desorption processes. The XPS results are shown in figure 8. In figure 8, after the sample was cycled at 30 °C under impure H_2 , the binding energies for P_1 and P_2 are 851.94 and 855.37 eV, corresponding to the Ni 2P_{3/2} and NiO 2P_{3/2}, respectively (<http://srdata.nist.gov/xps/>). For the 80 °C cycling, the binding energies for P_1 and P_2 are 852.21 and 855.58 eV, which is also consistent with the Ni 2P_{3/2} and NiO 2P_{3/2}, respectively (<http://srdata.nist.gov/xps/>). XPS

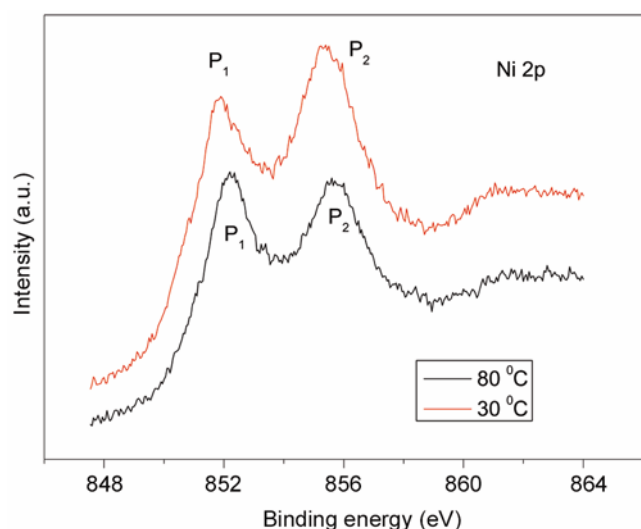


Figure 8. XPS spectra of the surface for element Ni.

results show that no nickel carbonyl was formed during the hydriding processes, indicating that CO appears to form a simple chemisorbed monolayer by adsorption rather than form nickel carbonyl.

3.4 TG and DTA analyses

Figure 9 shows the TG + DTA curves of the poisoned $\text{LaNi}_{4.7}\text{Al}_{0.3}$. In order to further investigate the reasons for $\text{LaNi}_{4.7}\text{Al}_{0.3}$ alloy hydrogen absorption capacity decrease at 30 °C, however, its performance is almost not changed at 80 °C in $\text{H}_2 + 300$ ppm CO, TG and DTA experiments on the poisoned sample were carried out. The results are shown in figure 9. Within the experimental temperature range of 30–150 °C, the sample weight loss is about 1.3%. Combining hydrogen absorption and desorption kinetic curves (figures 4 and 5), it is believed that the weight loss is mainly due to the release of hydrogen and a small amount of CO desorption from the alloy surface. Han and Lee (1989) also reported that gases released from the poisoned sample in the process of thermal decomposition contain CO, consistent with our results. In addition, it can be seen from figure 9 that the peak temperature for DTA is 76 °C, with a broad area. This is mainly attributed to CO desorption taking some time, indicating that the whole thermal decomposition process is accompanied by the CO desorption, which occurs simultaneously with hydrogen release.

As explained above, hydrogen absorption capacity decay at 30 °C is mainly because hydrogen molecules absorption and release are stopped by the adsorbed CO molecules, along with the undecomposed hydride presence. In this paper, hydrogen absorption and desorption were carried out under constant 80 °C temperature, which is consistent with the peak temperature of 76 °C. It is already known that Ni adsorbs CO by simple chemisorption, so hydrogen absorption at higher pressure will be beneficial for CO adsorption on the surface. However, when hydrogen desorbs at 80 °C in vacuum, the poisoned $\text{LaNi}_{4.7}\text{Al}_{0.3}$ alloy will self-recover (Sandrock and

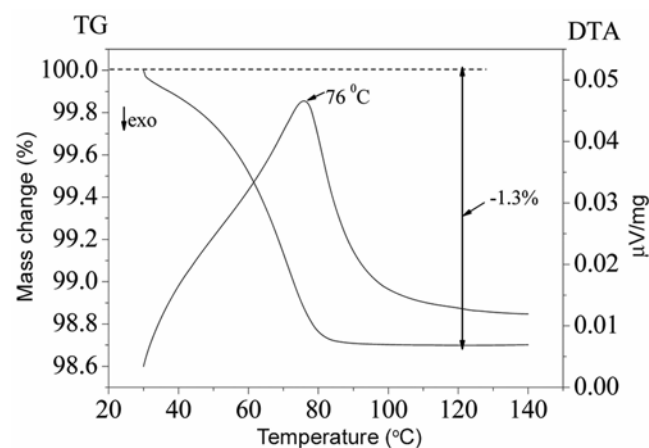


Figure 9. TG and DTA curves of the poisoned $\text{LaNi}_{4.7}\text{Al}_{0.3}$.

Goodell 1980), taking into account the peak temperature of 76 °C. Then, CO desorbs from the surface, followed by hydrogen desorption and complete release. Hence, in figure 5, no decrease in hydrogen absorption capacity was observed, opposite to hydrogen absorption at 30 °C. Since CO desorbs from the alloy surface during each hydrogen desorption cycle, the alloy surface remains clean from CO for the next hydrogen adsorption cycle. When CO comes in contact with the alloy particles in the next cycle, chemisorption process is repeated, along with the metallic Ni precipitation, causing more time for the first step to complete.

4. Conclusions

LaNi_{4.7}Al_{0.3} alloy almost does not absorb hydrogen after only 3 cycles in mixed gases of H₂ + 300 ppm CO at 30 °C, opposite to 80 °C. XRD results show that the same LaNi₅ main phase forms in the LaNi_{4.7}Al_{0.3} alloy after 80 °C cycle in both pure and impure H₂, while LaNi₅H₆ phase forms after 30 °C cycling in mixed gases. The absorption/desorption curves and XRD patterns show that the poisoning mechanism for CO is mainly because it deactivates the alloy surface and thus hinders hydriding and dehydriding processes. XPS results confirmed that Ni and CO form by a simple chemisorption process, rather than form nickel carbonyl. Combining TG, DTA and XRD results with hydrogen absorption/desorption kinetics curves, the characteristics of absorption/desorption kinetics for LaNi_{4.7}Al_{0.3} alloy at 80 °C under H₂ + 300 ppm CO can be summarized as follows:

- (I) Hydrogen absorption capacity for the activated sample did not decrease significantly after 7 cycles under impure hydrogen, mainly attributed to the experiment temperature.
 (II) The activated sample exhibited two different steps in the absorption curves, when cycled in H₂ + 300 ppm CO. The first step corresponds to the absorption of CO on Ni with a slower hydriding rate. The second step is attributed to Ni acting as a catalyst in the H₂ → 2H process with a rapid hydriding rate.

Acknowledgements

This work was financially supported by the Research Cooperation Project of Guangdong Province and the Ministry of Education (2009B090300147) and the National High-Tech R&D Program (863 Program) of China (2006AA05Z132).

References

- Au M, Chen C-G, Ye Z, Fang T-S, Wu J and Wang O-D 1996 *Int. J. Hydrogen Energy* **21** 33
 Cássia Colman R D, Torres L A, De Lima A F F and Appel L G 2009 *Int. J. Hydrogen Energy* **34** 9832
 Corré S, Gotoh Y, Sakaguchi H, Fruchart D and Adachi G-Y 1997 *J. Alloys Compd.* **255** 117
 David E and Kopac J 2011 *Int. J. Hydrogen Energy* **36** 4498
 Dunikov D, Borzenko V and Malyschenko S 2012 *Int. J. Hydrogen Energy* **37** 13843
 Eisenberg F G and Goodell P D 1983 *J. Less-Common Met.* **89** 55
 Goodell P D 1983 *J. Less-Common Met.* **89** 45
 Han J-I and Lee J-Y 1989 *J. Less-Common Met.* **152** 319
<http://srdata.nist.gov/xps/>
 Hwang K-R, Ryi S-K, Lee C-B, Lee S-W and Park J-S 2011 *Int. J. Energy Res.* **36** 10135
 Ibeh B, Gardner C and Ternan M 2007 *Int. J. Hydrogen Energy* **32** 908
 Imoto T, Satoh K, Nishimura K, Yonesaki T, Fujitani S and Yonezu I 1995 *J. Alloys Compd.* **233** 60
 Kosmambetova G R, Moroz E M, Guralsky A V, Pakharukova V P, Boronin A I, Ivashchenko T S et al 2011 *Int. J. Hydrogen Energy* **36** 1271
 Lototsky M V, Williams M, Yartys V A, Klochko Y V and Linkov V M 2011 *J. Alloys Compd.* **509S** S555
 Majlan E H, Wan Daud W R, Iyuke S E, Mohamad A B, Kadhum A, Amir H, Mohammad A et al 2009 *Int. J. Hydrogen Energy* **34** 2771
 Mendelsohn M H, Gruen D M and Dwight A E 1977 *Nature* **269** 45
 Mendes D, Chibante V, Zheng J-M, Tosti S, Borgognoni F, Mendes A et al 2010 *Int. J. Hydrogen Energy* **35** 12596
 Miura S, Fujisawa A and Ishida M 2012 *Int. J. Hydrogen Energy* **37** 2794
 Ren J, Williams M, Lototsky M, Davids W and Ulleberg Ø 2010 *Int. J. Hydrogen Energy* **35** 8626
 Sakaguchi H, Tsujimoto T and Adachi G 1995 *J. Alloys Compd.* **223** 122
 Sandrock G D and Goodell P D 1984 *J. Less-Common Met.* **104** 159
 Sandrock G D and Goodell P D 1980 *J. Less-Common Met.* **73** 161
 Schlapbach L, Seiler A, Stucki F and Siegmann H C 1980 *J. Less-Common Met.* **73** 145
 Scura F, Barbieri G, Luca G D and Drioli E 2008 *Int. J. Hydrogen Energy* **33** 4183
 Sheridan III J J, Eisenberg F G, Greskovich E J, Sandrock G D and Huston E L 1983 *J. Less-Common Met.* **89** 447
 Sun Y-M and Suda S 2002 *J. Alloys Compd.* **330-332** 627
 Tagliabue M and Delnero G 2008 *Int. J. Hydrogen Energy* **33** 3496
 Tosti S, Bettinali L and Violante V 2000 *Int. J. Hydrogen Energy* **25** 319
 Uchida H 1999 *Int. J. Hydrogen Energy* **24** 861
 Van Vucht J H N, Kuijpers F A and Bruning H C A M 1970 *Philips Res. Rep.* **25** 133
 Wallace W-E, Karlček R-F and Imamura Jr H 1979 *J. Phys. Chem.* **83** 1708
 Wang X-L, Iwata K and Suda S 1995 *J. Alloys Compd.* **231** 860
 Williams M et al 2009 *Mater. Chem. Phys.* **115** 136
 Williams M, Lototsky M V, Linkov V M, Nechaev A N, Solberg J K and Yartys V A 2009 *Int. J. Energy Res.* **33** 1171
 Xie D-H, Li P, Zeng C-X, Sun J-W and Qu X-H 2009 *J. Alloys Compd.* **478** 96
 Zhao X Y, Ding Y, Yang M and Ma L Q 2008 *Int. J. Hydrogen Energy* **33** 81